Role of triadin in the organization of reticulum membrane at the muscle triad.

Anne Fourest-Lieuvin, John Rendu, Alexis Osseni, Karine Pernet-Gallay, Daniella Rossi, Sarah Oddoux, Julie Brocard, Vincenzo Sorrentino, Isabelle Marty, Julien Fauré

Role of triadin in the organization of reticulum membrane at the muscle triad

Anne Fourest-Lieuvin[1,3,4], John Rendu[1,3,6], Alexis Osseni[1,3], Karine Pernet-Gallay[2,3], Daniella Rossi[5], Sarah Oddoux[1,3], Julie Brocard[1,3], Vincenzo Sorrentino[5], Isabelle Marty[1,3] and Julien Fauré[1,3,6,*]

[1]INSERM U836, Grenoble Institut des Neurosciences, Equipe Muscle et Pathologies, Grenoble 38042, France
[2]INSERM U836, Grenoble Institut des Neurosciences, Plateforme de Microscopie Electronique, Grenoble 38042, France
[3]Université Joseph Fourier, 38400 Saint-Martin-d'Hères, Grenoble, France
[4]Institut de Recherches en Technologies et Sciences pour le Vivant, Direction des Sciences du Vivant, CEA, 92265 Fontenay-aux-Roses cedex, France
[5]Molecular Medicine Section, Department of Neuroscience, and Interuniversity Institute of Myology, University of Siena, Siena 53100, Italy
[6]Centre Hospitalier Régional Universitaire de Grenoble, Hôpital Michallon, Biochimie et Génétique Moléculaire, La Tronche, Grenoble 38700, France
*Author for correspondence (julien.faure@ujf-grenoble.fr)

Accepted 27 March 2012
Journal of Cell Science 125, 3443–3453

doi: 10.1242/jcs.100958

Summary

The terminal cisternae represent one of the functional domains of the skeletal muscle sarcoplasmic reticulum (SR). They are closely apposed to plasma membrane invaginations, the T-tubules, with which they form structures called triads. In triads, the physical interaction between the T-tubule-anchored voltage-sensing channel DHPR and the SR calcium channel RyR1 is essential because it allows the depolarization-induced calcium release that triggers muscle contraction. This interaction between DHPR and RyR1 is based on the peculiar membrane structures of both T-tubules and SR terminal cisternae. However, little is known about the molecular mechanisms governing the formation of SR terminal cisternae. We have previously shown that ablation of triadins, a family of SR transmembrane proteins that interact with RyR1, induced skeletal muscle weakness in knockout mice as well as a modification of the shape of triads. Here we explore the intrinsic molecular properties of the longest triadin isoform Trisk 95. We show that when ectopically expressed, Trisk 95 can modulate reticulum membrane morphology. The membrane deformations induced by Trisk 95 are accompanied by modifications of the microtubule network organization. We show that multimerization of Trisk 95 by disulfide bridges, together with interaction with microtubules, are responsible for the ability of Trisk 95 to structure reticulum membrane. When domains responsible for these molecular properties are deleted, anchoring of Trisk 95 to the triads in muscle cells is strongly decreased, suggesting that oligomers of Trisk 95 and microtubules contribute to the organization of the SR terminal cisternae in a triad.

Key words: Triadin, Muscle, Reticulum, Calcium release, Triad, Microtubule

Introduction

Skeletal muscle contraction is achieved when an efficient depolarization of the sarcolemma triggers massive calcium efflux out of the sarcoplasmic reticulum (SR). This process called excitation-contraction (E–C) coupling relies on the physical interaction between two calcium channels that are anchored in different membrane compartments of the muscle cell (Block et al., 1994; Marty et al., 1994). The dihydropyridine receptor (DHPR) is present in invaginations of the plasma membrane, called transverse tubules (T-tubules), and the ryanodine receptor (RyR1) is located in cisternae of SR closely apposed to T-tubules. This unique membrane system, composed of two SR cisternae apposed to one T-Tubule, is called a triad and forms the basal structural unit responsible for E–C coupling (Flucher, 1992). Triads are evenly distributed along skeletal muscle cell longitudinal axis, and precisely localized in regard of each A–I transitions in sarcomeres. Numerous studies have highlighted the very high degree of organization of triad membranes that allows the physical interaction between the DHPR and RyR1 (Flucher and Franzini-Armstrong, 1996). It is therefore not surprising that deletion of several proteins of the SR cisternae induces modifications of the morphology of the triad that are associated to muscle cell dysfunction. For instance, mice knocked-out for junctophilin-1, a protein bridging SR to the plasma membrane, die at birth from feeding default and show reduced and disorganized triads in skeletal muscle (Ito et al., 2001). Ablation of the calsequestrin-1 protein, which binds calcium inside SR cisternae lumen, also impairs muscle function and induces modifications of the structure and composition of triads (Paolini et al., 2007). Although the specific structure of the triad membranes seems essential to sustain E–C coupling, the molecular determinants of SR cisternae morphology inside a triad are still largely unknown. A number of proteins associated with RyR1 in a macromolecular complex, the calcium release complex (CRC), have been shown to participate in the E–C coupling process, and could be candidates as molecular determinants of the shape of SR cisternae. The transmembrane Trisk 95 protein is one of these candidates.

Trisk 95 is one of the isoforms arising from alternative splicing of the *TRDN* gene (Thevenon et al., 2003). It is specifically expressed in striated muscle and exclusively localized at the triad (Brandt et al., 1990; Kim et al., 1990). The four triadin isoforms so far described are type II transmembrane proteins of different molecular mass (from 95 to 32 kDa) that share a common

cytosolic N-terminus and a single transmembrane domain. Their respective intra-luminal parts diverge by their lengths and by their last C-terminal amino acids. All the experiments based on modifications of the expression level of triadins have not allowed a clear view of their role in the calcium release process. When Trisk 95 was overexpressed in primary cultures of rat skeletal myotubes using adenovirus gene transfer, it resulted in a blocking of the depolarization-induced calcium release (Rezgui et al., 2005). A reduction of triadin expression by siRNAs in C2C12 myotubes resulted also in a partial inhibition of the depolarization-induced calcium release (Wang et al., 2009). Mice knocked-out for the triadin gene exhibited a reduced amount of stored calcium in muscle SR as well as a reduction in the depolarization-induced calcium release (Shen et al., 2007), associated with a marked reduction in muscle strength (Oddoux et al., 2009). Hence, in all these experiments, both an increased and a decreased expression of Trisk 95 resulted in similar observations, limiting interpretations on the real role of triadin in the E–C coupling.

We have observed by electron microscopy significant structural deformations of the triads in skeletal muscles of triadin KO mice (Oddoux et al., 2009). Therefore, we raised the hypothesis that Trisk 95 could play a role on the membrane structure of SR terminal cisternae in triads. To study the intrinsic properties of the Trisk 95 molecule regarding reticulum membranes, we have investigated its behavior after expression in a cell model devoid of muscle proteins. Our work shows that Trisk 95 expression in COS-7 cells induces a striking deformation of the endoplasmic reticulum (ER), together with modifications of the microtubule network morphology and dynamics. We have characterized the functional domains of Trisk 95 responsible for these phenotypes, and altogether our data suggest that triadin is involved in regulating the morphology of the SR membrane at the triad.

Results

Expression of Trisk 95 in COS-7 cells leads to ER membrane deformation

To investigate the properties of triadin regarding reticulum membranes, Trisk 95 was expressed in cultured COS-7 cells. In transfected cells, Trisk 95 staining showed three types of phenotype: (1) limited perinuclear sheets together with peripheral reticulated tubes, typical for ER (Fig. 1A, 'normal ER'); (2) sheets of membranes expanding to the cell periphery (Fig. 1A, 'large sheets'), and (3) rope-like structures emerging from perinuclear sheets that can be large or extremely compacted (Fig. 1A, 'ropes', arrowheads). Trisk 95 labeling colocalised with the endogenous ER marker calnexin, even when cells show the most dramatic phenotype (Fig. 1C), demonstrating that Trisk 95 expressed in COS-7 localizes in the ER and can induce ER membrane deformations. The apparition of ER rope-like structures correlated with an increase in the relative expression levels of Trisk 95 in cells (Fig. 1B), indicating that accumulation of Trisk 95 can modify reticulum membrane morphology. Such a phenotype has already been described for proteins known to regulate ER morphology (Klopfenstein et al., 1998; Park et al., 2010). To better characterize the reorganization of ER membranes observed after Trisk 95 expression, immuno-electron microscopy was performed on COS-7 cells expressing Trisk 95 fused to GFP (T95-GFP). The addition of GFP did not modify the ability of Trisk 95 to deform ER as detected by confocal microscopy (supplementary material Figs S2, S3, control). In immuno-electron microscopy, gold particles labeling T95-GFP were concentrated on narrow tubules delimitated by a lipid bilayer (Fig. 1D, arrowheads). These tubules show a striking reduction in diameter (39.4±0.27 nm) when compared to rough ER normal tubule diameter (63.52±2.19 nm) measured on untransfected cells.

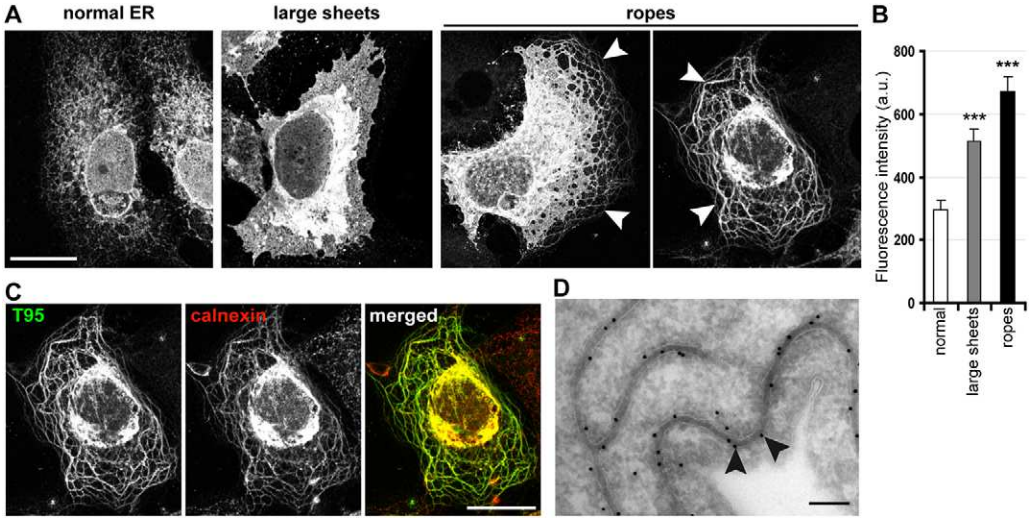

Fig. 1. Trisk 95 localizes in the ER and induces ER malformation. Trisk 95 was expressed in COS-7 cells for 28 hours before cell fixation and permeabilization. (**A**) Cells were stained with an antibody against the C-terminus of Trisk 95. Three patterns of Trisk 95 staining could be observed: a reticular pattern resembling normal ER, large sheets, and ropes (arrowheads). Scale bar: 20 μm. (**B**) Quantification of the mean fluorescence intensity for cells exhibiting each pattern. ***$P<0.001$, *t*-test comparisons of 'large sheets' ($n=20$ cells) or 'ropes' ($n=13$ cells) phenotype vs 'normal ER' ($n=12$ cells) phenotype. Error bars are s.e.m. (**C**) Cells expressing Trisk 95 were co-stained with antibodies against Trisk 95 (T95, green) and calnexin (red). Calnexin colocalized with Trisk 95, showing that ropes and sheets were ER compartments. Scale bar: 20 μm. (**D**) Electron microscopy image of a COS-7 cell expressing Trisk-95-GFP and labeled with immunogold. Membrane tubules with a narrow and regular diameter are labeled with the gold particles (arrowheads). Scale bar: 200 nm.

These data indicate that accumulation of Trisk 95 in the ER of non-muscle cells leads to drastic modifications of the ER membrane structure, especially tubular deformations referred to as 'rope-like structures'. Such ER rope-like structures have already been observed in association with a reorganization of the microtubule network (Vedrenne and Hauri, 2006). We have therefore investigated microtubules in Trisk-95-expressing cells.

Trisk-95-induced ER deformation is associated with a disorganization of the microtubule network

Trisk 95 transfected cells were co-labeled with anti-tubulin antibodies, and confocal images showed that rope-like structures positive for Trisk 95 co-aligned with microtubules (Fig. 2A). In transfected cells, microtubules appeared disorganized and bundled, with a loss of their normal radial pattern (Fig. 2B, arrowheads; quantification in Fig. 2C). To demonstrate microtubule bundling, we used correlative microscopy: cells transfected with T95-GFP were selected under a confocal microscope thanks to a carbon grid coated coverslip, and next analyzed by electron microscopy after appropriate fixation. Fig. 2G shows that microtubules observed in electron microscopy are clearly associated in bundles (arrowheads) in cells expressing T95-GFP. Bundling of microtubules is generally associated with a modification of the overall microtubule dynamics. This was tested by measuring the susceptibility of microtubules to the depolymerizing drug nocodazole in Trisk-95-expressing cells (Fig. 2D). In untransfected cells, only a few microtubules resisted a 30 minute nocodazole treatment (arrow). In contrast, bundled microtubules associated with Trisk-95-induced rope-like structures were not affected by the drug,

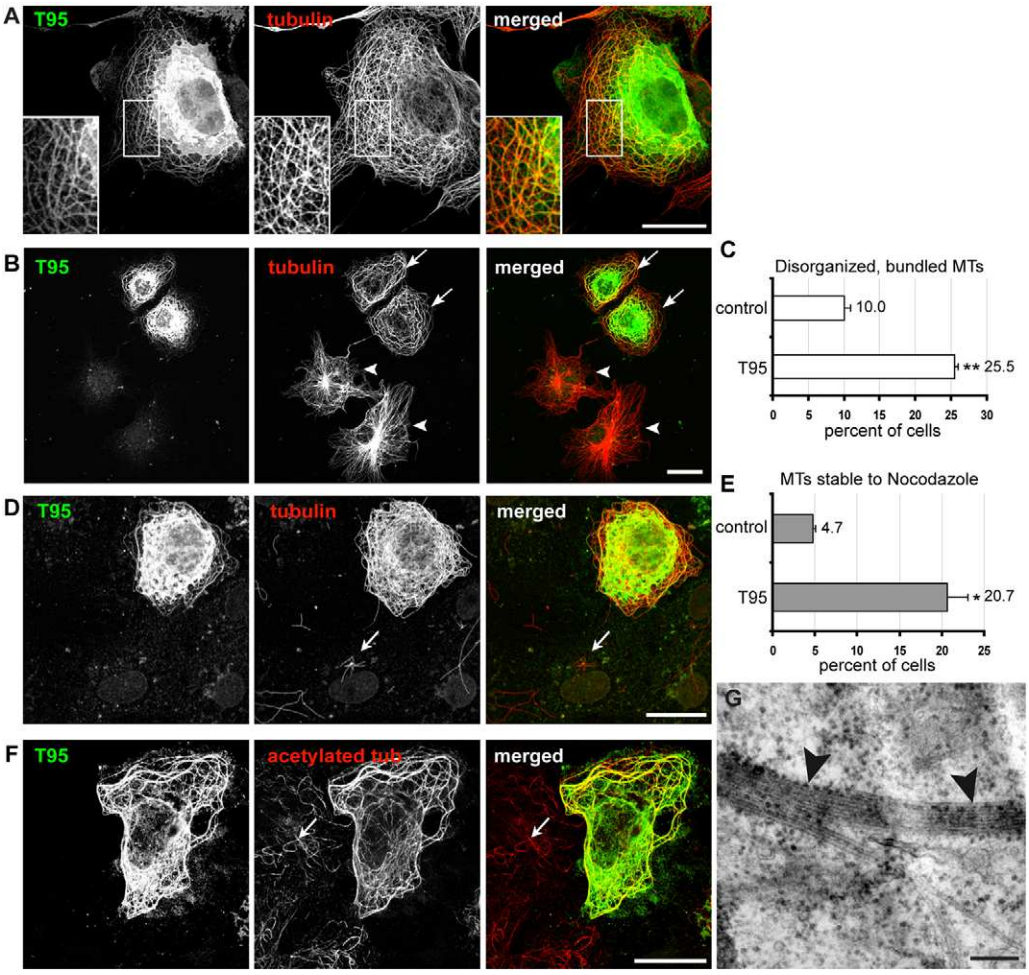

Fig. 2. ER ropes induced by Trisk 95 disorganize and stabilize microtubules. Trisk 95 was expressed in COS-7 cells. (**A**,**B**,**D**) Cells were co-stained with antibodies against Trisk 95 (T95, green) and β-tubulin (red). Scale bars: 20 μm. (A) ER ropes induced by Trisk 95 expression colocalize with microtubules (see zooms in insets). (B) Cells expressing Trisk 95 show disorganization and bundling of microtubules (arrows), which is not the case in non-expressing cells (arrowheads). (**C**) Quantification of cells with disorganized microtubules, in non-transfected (control) cells and in T95-expressing cells. $^{**}P<0.01$, *t*-test comparisons of T95-transfected cells vs control. Error bars are s.e.m.; $n=3$ experiments. (**D**) After 28 hours of Trisk 95 expression, cells were treated with nocodazole and then lysed. In T95-expressing cells, most microtubules resisted nocodazole treatment, whereas in non-transfected cells, only a few microtubules remained (arrow). (**E**) Quantification of cells exhibiting a large array of stable microtubules, in non-transfected (control) cells and in T95-expressing cells. $^{*}P<0.05$, *t*-test and error bars as in C. (**F**) Cells were co-stained with antibodies against Trisk 95 (green) and acetylated tubulin (red). In non-transfected cells, only a few microtubules were acetylated (arrow), whereas T95-transfected cells exhibited massive acetylation of microtubules. Scale bar: 20 μm. (**G**) COS-7 cells expressing T95-GFP were processed for correlative electron microscopy to visualize microtubules. Microtubules were often found as bundles (arrowheads) in the cytosol of these cells. Scale bar: 200 nm.

indicating they have a slower turnover (quantification in Fig. 2E). To confirm this alteration in the microtubule dynamics, we used an antibody specific for acetylated-tubulin, a post-translationally modified form of tubulin that is present preferentially in stabilized microtubules. Fig. 2F shows that bundles of microtubules generated by Trisk 95 expression are extensively labeled by the anti-acetylated tubulin antibody. In untransfected cells, only a subset of the microtubule network is labeled (arrow). These results demonstrate that expression of Trisk 95 in COS-7 cells modifies microtubule network organization as well as microtubule dynamics.

Trisk 95 interacts with microtubules

Deformations of ER membranes into rope-like structures that are aligned along bundled microtubules are the hallmarks of proteins that can bridge both organelles. Two proteins described as directly regulating ER membrane morphology, Climp-63 and REEP1, also interact with microtubules (Klopfenstein et al., 1998; Park et al., 2010). Both proteins, when overexpressed in COS cells, lead to the same phenotype as that observed for Trisk 95. We therefore tested whether Trisk 95 could also interact with microtubules using a co-sedimentation assay (Fig. 3A). HEK293 cells showed rope-like structures when transfected with Trisk 95 (supplementary material Fig. S1) and were used to obtain large amounts of Trisk-95-enriched lysates (Fig. 3A, lane L). Trisk-95-enriched lysates were incubated with purified tubulin in conditions allowing the polymerization of microtubules, which were then sedimented by centrifugation trough a glycerol cushion. In the resulting pellet (P1), microtubule-associated proteins were discriminated from aggregates by a depolymerization step of the microtubules: proteins interacting with microtubules were released together with free tubulin (lane MT) whereas aggregates were pelleted by a second centrifugation (lane P2). Fig. 3A shows that Trisk 95 was present in the P2 fraction after this co-sedimentation assay, suggesting that it aggregated. This aggregation of the protein hindered the detection of any potential interaction with microtubules. Previous work in skeletal muscles had underlined that Trisk 95 was able to form large multimeric complexes, probably mediated by disulfide bridges (Froemming et al., 1999). To disrupt these complexes that could account for Trisk 95 sedimentation in the P2 pellet, we generated a mutant form of Trisk 95 where both cysteines of the molecule were replaced by alanines (Trisk 95 2C>A). Fig. 3B shows that indeed mutation of both cysteines of Trisk 95 to alanines is sufficient to abolish multimerization of the protein, as observed by non-denaturing electrophoresis (compare lanes 1 and 4). The Trisk 95 2C>A mutant was therefore used in a microtubule co-sedimentation assay (Fig. 3C), and a significant proportion of the Trisk 95 2C>A protein was found co-sedimenting with the microtubules (MT fraction). This indicated that Trisk 95, which is a transmembrane ER protein, could interact with the microtubules, suggesting that the formation of rope-like structures might rely on the microtubule network. We next investigated the effect of microtubule-stabilizing and -depolymerizing agents on the formation of ER rope-like structures. When COS-7 cells transfected with Trisk 95 were treated with Taxol, rope-like structures appeared rigidified, following exactly the microtubule pattern induced by the stabilizing agent (supplementary material Fig. S2). Moreover, we also showed that rope-like structures disappeared after a 2 h incubation time with nocodazole (supplementary material Fig. S3). Thus, reticulum membranes deformed by Trisk 95 expression follow microtubule tracks, and require an intact microtubule network to be maintained.

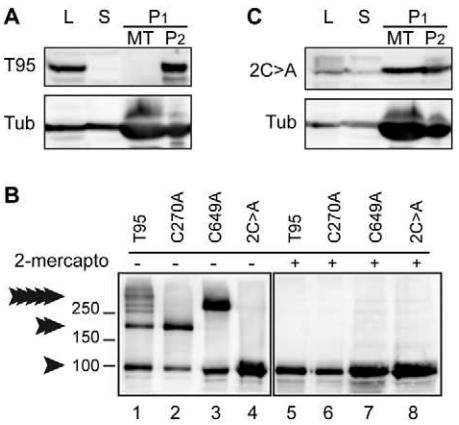

Fig. 3. Trisk 95 can bind microtubules when devoid from its two cysteine residues that mediate oligomerization. Wild-type Trisk 95 (T95) or Trisk 95 mutated on one (C270A or C649A mutant) or both luminal cysteines (mutant 2C>A), were expressed in HEK293 cells before cell lysis. (**A**,**C**) Lysates (L) were processed for microtubule co-sedimentation assay: they were incubated at 37℃ with tubulin, GTP and Taxol to induce microtubule polymerization, and centrifuged on a glycerol cushion to separate the supernatant not associated with microtubules (S) from the microtubule pellet (P1). Microtubules in this pellet were depolymerized and centrifuged again to separate true microtubule fraction (MT) from a pellet of protein complexes or aggregates (P2). Fractions were processed for SDS-PAGE and western blotting with antibodies against Trisk 95 (top panels) and β-tubulin (bottom panels). Trisk 95 is in the P2 fraction, showing that it either aggregates or forms protein complexes, whereas the 2C>A mutant is mostly present in the MT fraction, associated with microtubules. (**B**) Cysteines 270 and 649 mediate oligomerization of Trisk 95. Cell lysates were processed for SDS-PAGE either with non denaturing or denaturing sample buffers (with or without mercaptoethanol), followed by western blotting with an antibody against Trisk 95. In non-denaturing conditions, a monomeric form of 95 kDa (>), a dimeric form of about 200 kDa (>>) and multimeric forms (>>>>>) of Trisk 95 were visible (lane 1). For the 2C>A double mutant, only the monomeric form is present (lane 4). The monomeric form was present in both C270A and C649A simple mutants, but the dimeric form was visible only for the C270A mutant (lane 2) whereas the C649A mutant might form a hetero-oligomer with an unknown partner (band above 250 kDa, lane 3).

Altogether, our data show that Trisk 95 is able to (1) intensively modify ER membrane shape; (2) align these membranes onto microtubules; and (3) interact with microtubules. These features are characteristic of proteins recently described as regulators of reticulum membrane structure (Park and Blackstone, 2010) and to further investigate the molecular properties of Trisk 95, we searched for domains of the molecule responsible for ER and microtubule array deformation.

The luminal domain of Trisk 95 is responsible for ER and microtubule deformations

Trisk 95 has been described as a single pass transmembrane protein, with a long C-terminal luminal domain and a short N-terminal part facing the cytosol (Marty et al., 1995). Truncated versions of Trisk 95 were generated by deleting either the cytosolic part of the molecule (Fig. 4A, T95ΔN), or the luminal part starting from residue 114 (Fig. 4A, Tmini). Each of these constructs was expressed in COS-7 cells, and transfected cells

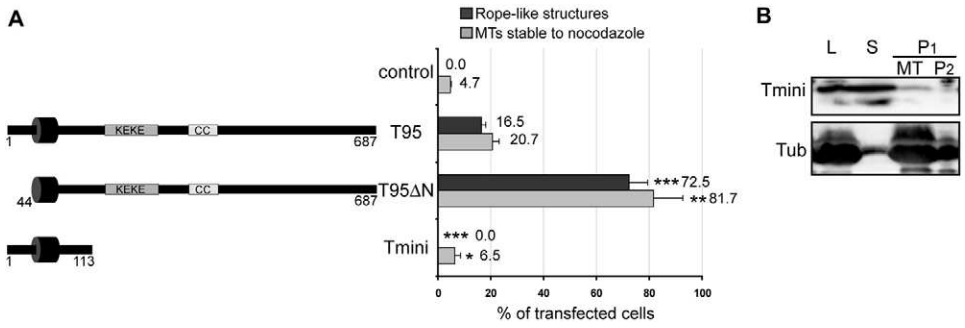

Fig. 4. The luminal part of Trisk 95 is responsible of ER deformation and microtubule stabilization. (**A**) COS-7 cells were transfected with Trisk 95 (T95) or with constructs of Trisk 95 deleted either for its 43 N-terminal residues (T95ΔN) or for most of its luminal part (Tmini). Sequences of Trisk 95 corresponding to the transmembrane domain (black box, aa 46–66), to the KEKE domain (aa 210–224) and to a coiled-coil domain (CC, aa 306–341) are depicted. After transfection, cells were either directly stained with an antibody against Trisk 95 to quantify the number of transfected cells exhibiting ER rope-like structures, or treated with nocodazole as in Fig. 2D to quantify the number of transfected cells showing microtubules stable to nocodazole. Quantifications were also performed on non-transfected cells (control). $*P<0.05$, $**P<0.01$, $***P<0.001$, *t*-test comparisons of T95ΔN or Tmini-transfected cells vs T95-transfected cells. Error bars are s.e.m., $n=3$ experiments. (**B**) Tmini mutant was processed for microtubule co-sedimentation assay as in Fig. 3. Tmini remains in the supernatant (S) fraction, showing that it does not bind microtubules.

exhibiting ER rope-like structures or microtubule stability after nocodazole treatment were quantified (Fig. 4A). Compared to wild-type Trisk 95, expression of the T95ΔN mutant increased drastically the number of cells with rope-like structures (from 16.5 to 72.5% of transfected cells), and with stable microtubules (from 20.7 to 81.7%). On the contrary, the Tmini construct did not induce any rope-like structure and had no impact on microtubule stability when compared to control cells (Fig. 4A). These results suggest that the luminal domain of Trisk 95 is required to generate ER and microtubule deformations. Moreover, deletion of the N-terminal part of Trisk 95 does not abolish the microtubule stabilization phenotype, suggesting that the N-terminus of Trisk 95, although facing the cytosol, is not directly interacting with the microtubule network. To confirm this, we used lysates of HEK293 cells expressing Tmini in the microtubule co-sedimentation assay. Fig. 4B shows that Tmini is not present in the microtubule fraction, and remains in the supernatant (S) after the first centrifugation, confirming that Trisk 95 does not interact with microtubules via its N-terminal domain, but rather through its C-terminal domain. Because Trisk 95 C-terminal domain is inside the luminal space of the ER, its interaction with microtubules must be indirect.

These experiments show that the luminal domain of Trisk 95 contains the motives responsible for its molecular properties. They also show that the deletion of the cytosolic part of Trisk 95 strongly enhances the occurrence of rope-like structures, as well as the stabilization of microtubules, suggesting that the cytosolic N-terminal part of Trisk 95 plays a regulatory role in the phenotypes we observe. We next dissected the lumenal part of Trisk 95 to define regions responsible for the properties of the molecule.

Two cysteines and a coiled-coil motif are responsible for molecular properties of Trisk 95

We have demonstrated that cysteine disulfide bridging is responsible for the formation of large multimeric complexes of Trisk 95 (Fig. 3B). Such platforms of molecules could modify the morphology of ER membranes in COS-7 cells. To investigate this hypothesis, we monitored ER morphology after expression of single cysteine mutants of Trisk 95, that could only make dimers (as shown in Fig. 3B, lanes 2 and 3), or double cysteine mutant, that is monomeric (Fig. 3B, lane 4). Fig. 5A shows that single cysteine mutant (C270A or C649A) expression induced a diminution of 50% of rope-like structure occurrence compared to wild-type Trisk 95, indicating that dimers of Trisk 95 are less prone to induce membrane deformations. Accordingly, the expression of the double cysteine mutant (2C>A) induced a supplemental 50% drop in the number of cells showing ER deformation. However, the localization of the 2C>A mutant was modified: instead of a unique intracellular reticulum staining, as observed for Trisk 95 C270A and C649A, we noticed that the 2C>A mutant also exhibited a plasma membrane labeling. By immunofluorescence studies, we showed that the 2C>A mutant can be detected on cells fixed without permeabilization with an antibody directed against the C-terminal part of the protein (Fig. 5B), which is not the case for wild-type Trisk 95. After permeabilization of the cells, both proteins are recognized with an antibody against the N-terminus of the molecule. To further demonstrate the plasma membrane localization of the 2C>A mutant, we realized a purification of cell surface proteins after biotinylation. The panel C of Fig. 5 shows that a significant proportion of the 2C>A mutant is recovered in the plasma membrane fraction (Mb, lane 5), in contrast to the WT form of Trisk 95 (Mb, lane 3).

Single cysteine mutants showed a marked reduction in the formation of rope-like structures, thus suggesting that multimerization of Trisk 95 could be responsible for ER membrane deformation. Mutation of the 2 cysteines residues of Trisk 95 induces its exit of the ER and may explain partially why the 2C>A mutant shows much less rope-like structure than wild-type Trisk 95. However, the 2C>A mutant still present in the ER was able to induce a few rope-like structures, suggesting that other sequences of the molecule are also responsible for ER membrane deformations. We focused on two motives of interest: (1) a highly charged stretch of lysines and glutamate, called the KEKE motif (aa 210 to 224) (Realini et al., 1994), that allows interaction of triadins with RyR1 and calsequestrin (Kobayashi et al., 2000; Lee et al., 2004) and (2) a putative coiled-coil motif

(aa 306 to 341) which was detected with COILS and PCOILS software (http://toolkit.tuebingen.mpg.de/pcoils). We generated in-frame deletions of these motives, individually (mutants Δ114–264 and Δ306–341) or together (mutant Δ114–341), and expressed them in COS-7 cells. We showed that the deletion of the small coiled-coil motif (Δ306–341) was sufficient to induce a 53% reduction (from 16.5% to 7.8% of transfected cells) in the generation of rope-like structures (Fig. 5D).

Therefore, a putative coiled-coil domain and cysteine residues are responsible for the ER membrane deformations generated by Trisk 95. In order to confirm this, we generated a version of Trisk 95 with 2C>A and Δ306–341 mutations (T95 Δ306–341 2C>A). As shown in Fig. 5D, this mutant form of Trisk 95 induced ER deformation in as few as 2.1% of transfected COS-7 cells. The effect of each mutation seems therefore additive to the other, suggesting that ER membrane deformation we observe may depend on two different mechanisms requiring both coiled-coil domain and disulfide bridging in Trisk 95.

We thus revealed, using COS-7 cells, domains that could account for the Trisk 95 molecular properties: indirect interaction with the microtubule network and modulation of reticulum membrane morphology. In the skeletal muscle, these properties could play a role in the structure and function of SR membrane in triads. We therefore tested whether triads in muscle cells could contact the microtubule network, and if Trisk 95 domains could be involved in the organization of sarcoplasmic reticulum membranes.

Muscle triads contact some microtubule tracks

In undifferentiated cells, reticulum membranes have been shown to make local contact points with the microtubule network (reviewed in Vedrenne and Hauri, 2006). However, in skeletal muscle, contacts between membranes of the terminal cisternae of SR and microtubules are poorly characterized. We performed double immunofluorescent labeling of triads and microtubules in isolated *flexor digitorum brevis* muscle of adult mouse (Fig. 6). Triads labeled by an anti-RyR1 antibody showed characteristic double rows of dots (Fig. 6, left images). The microtubules appear both in longitudinal and transversal orientation (Fig. 6, central images) as already reported (Ralston et al., 1999; Prins et al., 2009). Overlapping labeling of RyR1 and microtubules can be detected on the merged image of panel B as yellow dots. At higher magnification (panel C), triads labeling appear close to microtubules tracks, with a proportion of dots co-localizing with microtubules (Fig. 6C, arrowheads). This partial overlap between the labeling of triads and microtubules thus suggests the existence of some contact points between SR terminal cisternae and microtubules in muscles.

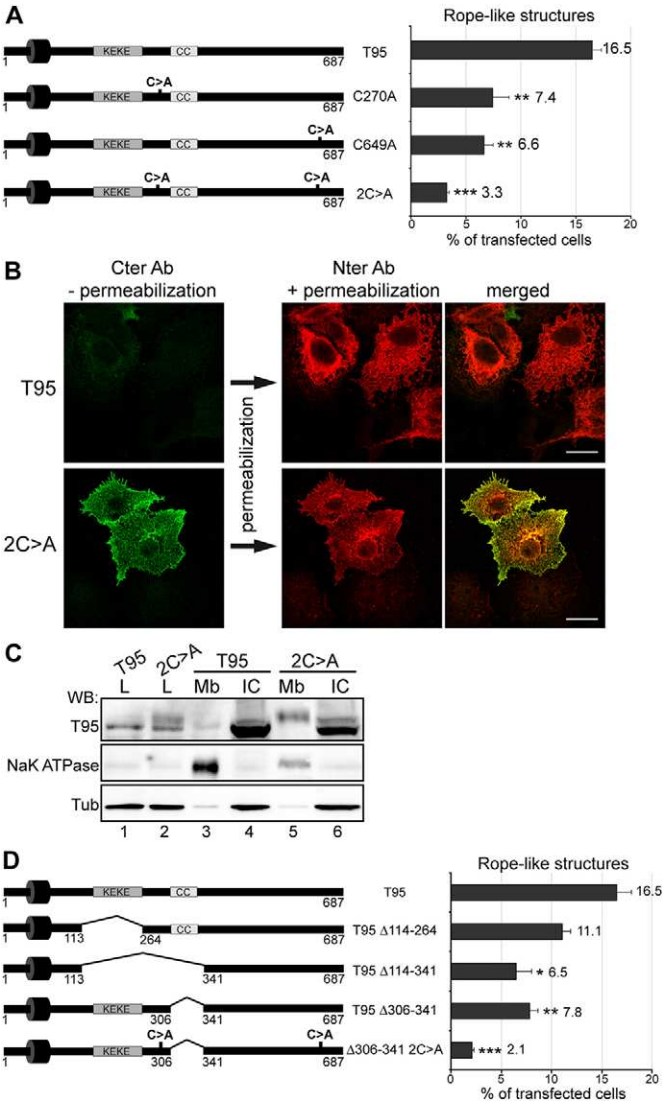

Fig. 5. Trisk 95 properties depend on its luminal cysteines and coiled-coil domain. (**A**) Wild-type Trisk 95 (T95) or Trisk 95 mutated on one (mutant C270A or C649A) or both luminal cysteines (mutant 2C>A), were transfected in COS-7 cells. After immunolabeling with an antibody against Trisk 95, transfected cells exhibiting ER rope-like deformations were counted. Sequences of Trisk 95 corresponding to the transmembrane domain (black box, aa 46–66), to the KEKE domain (aa 210–224) and to a coiled-coil domain (CC, aa 306–341) are depicted. $^{**}P<0.01$, $^{***}P<0.001$, *t*-test comparisons of mutants vs T95. Error bars are s.e.m.; $n=3$ experiments. (**B**,**C**) Mutation of both cysteines partly delocalizes Trisk 95 to the plasma membrane. (B) COS-7 cells were transfected either with Trisk 95 or with the double cysteine mutant 2C>A. Cells were fixed without permeabilization and stained with an antibody against the C-terminus of Trisk 95 (green), showing that only the 2C>A mutant localized at the plasma membrane. Afterwards, cells were permeabilized and stained with an antibody against the N-terminus of Trisk 95 (red) to reveal whole cell staining of wild-type or mutant Trisk 95. Scale bars: 20 μm. (C) COS-7 cells were transfected either with Trisk 95 or with the mutant 2C>A, and processed for biotinylation of cell surface proteins. Cells were then lysed (L fraction) and incubated with Streptavidin-coupled beads to trap biotinylated cell surface proteins (Mb fraction) and separate them from intracellular proteins (IC fraction). Each fraction was processed for SDS-PAGE and western blotting, the latter revealed either with an antibody against Trisk 95 (T95), or with an antibody against plasma membrane protein Na^+/K^+-ATPase, or with an antibody against cytosolic protein β-tubulin (Tub). Mutant 2C>A is present in the plasma membrane fraction (Mb, lane 5), and the observed increase in molecular mass is due to the coupling with the crosslinker. (**D**) Trisk 95 or the indicated deletion mutants of Trisk 95 were transfected in COS-7 cells and, after immunolabeling with an antibody against Trisk 95, transfected cells exhibiting ER rope-like structures were counted. The Δ306-341 2C>A mutant is deleted for the coiled-coil domain and mutated on both luminal cysteines. $^{*}P<0.05$, $^{**}P<0.01$, $^{***}P<0.001$, *t*-test comparisons of mutants vs T95. Error bars are s.e.m., $n=3$ experiments.

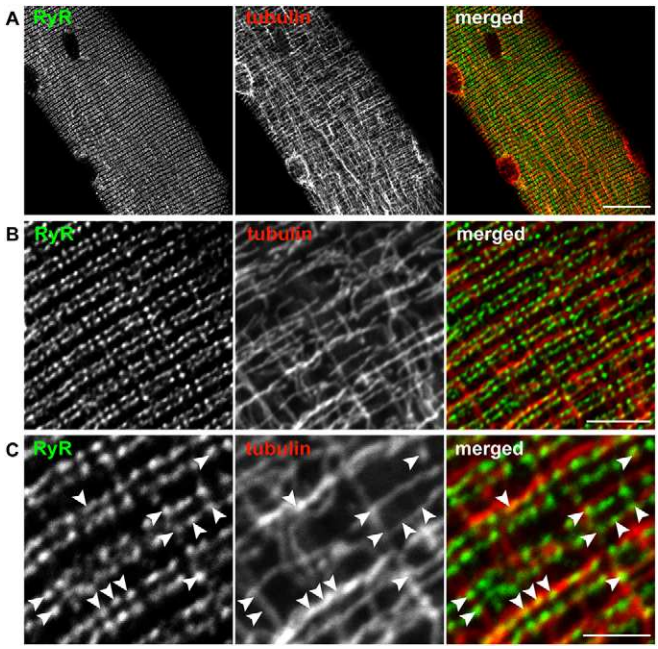

Fig. 6. In muscle cells, triads are often on microtubule tracks. (**A**) Isolated FDB muscle fibers were double-stained with an antibody against RyR1 to label triads (green) and with an antibody against β-tubulin to label microtubules (red). Each image represented one single confocal plane. (**B**,**C**) Zooms of the images in A. In C, arrowheads point to some of the triads that co-align with microtubules. Scale bars: 20 μm (A), 5 μm (B) and 2.5 μm (C).

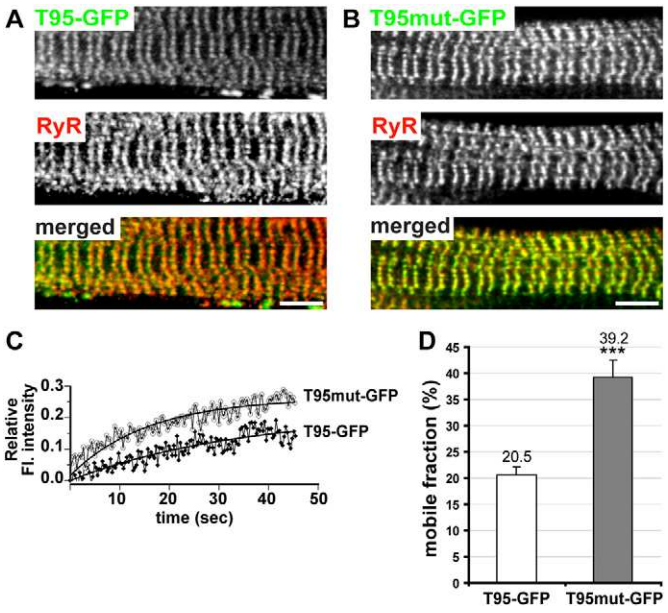

Fig. 7. In muscle cells, anchoring of Trisk 95 in triadic clusters depends on luminal cysteins and coiled-coil domain. (**A**,**B**) Primary rat myoblasts were transfected with expression vector for Trisk-95-GFP (T95-GFP in A) or Trisk 95 Δ306–341 2C>A (T95mut-GFP in B), and induced to differentiate for 12 days. Cells were counterstained with an antibody against RyR1. T95-GFP and T95mut-GFP (green) both colocalize with RyR1 (red) in triadic clusters. Scale bars: 5 μm. (**C**) Primary rat myoblasts were transfected with T95-GFP or T95mut-GFP and induced to differentiation as in A and B. FRAP analysis was performed on single triadic clusters. The relative fluorescence intensity was calculated after correction of background and loss of fluorescence with time. On the fluorescence recovery curves, time 0 is the time of photobleaching. (**D**) The mobile fraction for each protein was calculated from fluorescence recovery data. ***$P<0.001$, *t*-test comparisons of T95mut-GFP vs T95-GFP mobile fractions. Error bars are s.e.m.; $n=21$ clusters analyzed for each of the two proteins.

Cysteines and coiled-coil motif are responsible for Trisk 95 anchoring in muscle cell triads

In skeletal muscle, the mechanisms responsible for the exclusive localization of the proteins of the calcium release complex (CRC) in the terminal cisternae of the SR are not known. However, we have previously shown that the assembly of these proteins in clusters, before triad formation, is accompanied by a strong decrease in their mobility as measured by FRAP analysis (Cusimano et al., 2009). Among proteins of the CRC, Trisk 95 shows the most drastic reduction in mobility when reaching the triadic cluster, suggesting it plays a central role in the formation of a functional triad. The data presented above show that cysteine residues and a coiled-coil domain are responsible for Trisk 95 properties in COS-7 cells. Therefore, we tested if mutations of these domains affected Trisk 95 properties in triads of muscle cells. We expressed T95-GFP and the mutant Δ306–341 2C>A form of Trisk-95-GFP (T95mut-GFP) in cultured rat myotubes. Both constructs were detected in triads, where they colocalized with endogenous RyR1 (Fig. 7A,B). Their mobility in the SR membrane was compared by FRAP analysis performed on the triad clusters (Fig. 7C,D; supplementary material Fig. S4). The Δ306–341 2C>A mutant of T95-GFP exhibited a 90% increase in mobility compared to the wild-type T95-GFP (39.2±3.3 vs. 20.5±1.6). This result suggests that in muscle cells, cysteine residues and the coiled-coil domain of Trisk 95 favor the anchoring of Trisk 95 at the triad.

Discussion

In skeletal muscle, E–C coupling relies on the specific morphology of the triad membranes, which allows physical interaction between the DHPR and RyR1. However, mechanisms regulating the shape of SR cisternae closely apposed to plasma membrane T-tubules in a triad are largely unknown. Deletion of the DHPR and RyR1, which provide a physical link between SR cisternae and T-tubule, does not modify the correct organization of the triad (Flucher et al., 1992; Felder et al., 2002), thus suggesting that morphology of SR cisternae and T-tubule membranes are regulated by other factors. At the plasma membrane, the protein BIN1 regulates the formation of T-tubules by directly shaping lipid bilayers (Lee et al., 2002), and when expressed in COS-1 cells, BIN1 induces important plasma membrane deformations (Nicot et al., 2007). Regarding the regulation of SR cisternae morphology, mechanisms are less understood. Junctophilin has been described as a potential link between SR cisternae and T-tubules (Takeshima et al., 2000), and as such could be responsible for junctional SR membrane overall structure (Ito et al., 2001). Nevertheless, other proteins are also probably involved in the structure of SR membrane. Our results shed new light on the intrinsic properties of Trisk 95 and on its potential role in the organization of SR terminal cisternae.

We show that, when ectopically expressed, Trisk 95 modifies ER morphology, inducing rope-like structures and large ER sheets. These deformations are a hallmark of the overexpression of proteins responsible for ER morphology (Vedrenne and Hauri, 2006; Shibata et al., 2009; Park and Blackstone, 2010). Indeed,

rope-like structures have been first reported after overexpression of the ER protein Climp-63 (Klopfenstein et al., 1998). Large reticulum sheets have also been observed in cells with imbalanced proportions of Climp-63 and proteins of the reticulon family, which directly regulate the curvature of ER membranes (Shibata et al., 2010). Interestingly, it was shown that Climp-63 also interacts with microtubules (Klopfenstein et al., 1998). More recently, another protein proposed to contribute to ER shape, REEP1, was also shown to directly interact with microtubules (Park et al., 2010). Overexpression of these proteins generates ER membrane deformations, but also increases contact points between ER and microtubules, inducing a co-alignment between rope-like structures and microtubules. We demonstrate here that Trisk 95 expression induces the same phenotype as these proteins regarding ER and microtubule network deformations. Furthermore, Trisk 95 can interact with microtubules, but unlike REEP1 and Climp-63, this interaction is most probably indirect and mediated by its C-terminal luminal part. Our data on Trisk 95 seem to recapitulate phenotypes of proteins involved in the regulation of reticulum membrane morphology and argue in favor of a structural role for Trisk 95 on SR membranes at the triad of muscle cells.

Insights on the molecular mechanisms by which Trisk 95 could play such a role are provided by our exploration of functional domains of the molecule. We first abolished Trisk 95 oligomerization by mutation of its two cysteines, and this drastically reduced ER rope-like structure formation. This reduction could be explained, at least in part, by the modification of the subcellular localization of the mutated protein, a portion of which exiting the ER and reaching the plasma membrane. Interestingly, the morphology of the plasma membrane appeared normal in these cells after expression of this monomeric form of Trisk 95. This could mean that Trisk-95-induced deformations are specific of ER and not of plasma membrane. We have shown that mutations of single cysteines in Trisk 95 reduced by 50% its ability to generate rope like-structure, suggesting that oligomers containing more than two Trisk 95 are required to efficiently modulate ER membrane shape. Of note, proteins that directly modulate ER membrane morphology, like Climp-63, REEP1 and members of the reticulon family, are able to form large oligomers (Klopfenstein et al., 2001; Shibata et al., 2008; Park et al., 2010). Therefore, we hypothesize that oligomeric platforms of Trisk 95 could modify the reticulum membrane shape. Secondly, we showed that deletion of the coiled-coil domain of Trisk 95 reduced the formation of ER rope-like structures. This domain might therefore also be responsible for Trisk 95 molecular properties regarding membrane morphology, by mediating interactions with an ER resident protein, and favoring either membrane deformation or indirect interaction with microtubules. This putative partner of Trisk 95 is currently under investigation.

A role for Trisk 95 in the structure of the triad of skeletal muscle has been recently proposed (Marty et al., 2009). We showed previously that in muscles of mice knocked-out for the triadin gene, the orientation and the shape of the triad are modified (Oddoux et al., 2009). In addition, we showed that Trisk 95 integration into triads was accompanied by a drastic drop in its mobility as measured by FRAP analysis, and suggested that anchoring of Trisk 95 to the triad mediated by its C-terminal luminal part was a prerequisite to the building of the calcium release complex (Cusimano et al., 2009). Our present work suggests two roles for Trisk 95 at the triad: a bridging of the CRC to external structural cues, like the microtubule network, and a regulation of the SR triad membrane morphology.

First, we show here that Trisk 95 is able to interact with microtubules. Moreover, by confocal microscopy, we observe that some triads are aligned onto muscle cell microtubules, although not all the triads overlap with microtubules. This might reflect that (1) the SR membranes have a limited number of contact points with microtubules, as it is the case for ER membranes in undifferentiated cells (Vedrenne and Hauri, 2006) and (2) microtubule to SR membrane contacts are dynamic and hardly pinpointed in fixed cells. Nevertheless, these experiments argue in favor of a role for the microtubule network in the skeletal muscle E–C coupling, which is so far not studied. Of note, in cardiac muscle, microtubules disruption has already been reported to modulate calcium release (Gomez et al., 2000), and one of the possible roles of microtubules in cardiac E–C coupling could be to deliver proteins of the CRC at the dyads (Hong et al., 2010).

Second, we show in this work that deletion of the coiled-coil domain and the cysteine residues from the luminal part of Trisk 95 increases the mobility of Trisk 95 in muscle triads. This result confirms that these sequences are indeed functional domains of Trisk 95 in muscle cells and might contribute to its anchoring in SR membrane triad. Along these lines, we have previously shown that the shortest triadin isoform Trisk 32, which does not have these domains, is also expressed in skeletal muscle but is mainly localized in longitudinal SR membranes (Vassilopoulos et al., 2005). The coiled-coil domain and the cysteine residues could also contribute to modulate SR membrane shape. A recent study by cryo-electron tomography has shown that the lipid bilayers of the SR immediately surrounding the ryanodine receptor in isolated triads are highly curved (Renken et al., 2009), and this study argues in favor of an interplay between local membrane curvature and RyR1 function. Our immuno-electron microscopy data show that expression of Trisk 95 in the reticulum reduces the diameter of ER luminal space, and this could directly result from an enhanced ER membrane curvature.

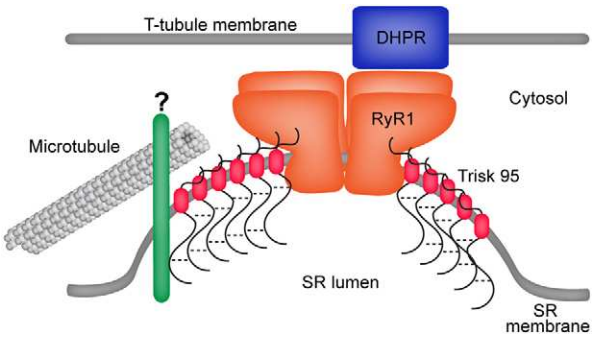

Fig. 8. Working model on the roles of Trisk 95 at the triad in muscle cells. Trisk 95, depicted with its transmembrane domain in red, is localized in the SR membrane and can bind RyR1 (depicted in orange) both via its N-terminal part and via the KEKE domain in its C-terminal luminal part. It can oligomerize via disulfide bridges (dotted lines), and can also bind an unknown partner (in green), which associates with microtubules (in grey). Oligomerization and indirect association with microtubules might mediate the anchoring of Trisk 95 at the SR junctional cisternae in the triad, and regulate the overall structure of the SR membrane in this region, favoring the coupling of RyR1 with the DHPR (in blue) localized in the T-tubule membrane.

Overall, we propose a working model for the role of Trisk 95 in skeletal muscle E–C coupling (Fig. 8). The oligomerization via disulfide bridging could generate platforms of Trisk 95 at the terminal cisternae of the SR. These oligomers may contribute to the local shaping of the SR membrane, which could regulate RyR1 function. Besides, triadin could mediate, via the coiled-coil domain, an interaction with an unknown SR protein linked to the microtubule network. This indirect link with the microtubules may favor the anchoring of the CRC proteins at the triad.

Materials and Methods

DNA constructs, expression vectors and antibodies

Full-length cDNA of rat triadin Trisk 95 inserted into the expression vector pcDNA3.1 (Invitrogen) has already been described (Marty et al., 2000). To construct Trisk-95-GFP, the stop codon of Trisk 95 in pcDNA3.1 was removed by a PCR-based method, and the amplified sequence was inserted into pEGFP-N1 (Clontech). The various Trisk 95 mutants were generated by site-directed mutagenesis using the Quikchange kit (Stratagene) or by PCR procedures that introduce either premature stop codons or restriction sites used to cut and ligate the modified sequence. DsRed2-ER plasmid was from Clontech. Primary antibodies used in this study are: guinea pig or rabbit polyclonal antibodies (pAbs) against the C-terminus of rat Trisk 95 (Vassilopoulos et al., 2005), rabbit pAb against the N-terminus of Trisk 95 (Vassilopoulos et al., 2005), rabbit pAb against RyR1 (Marty et al., 1994), rabbit pAb against calnexin (Stressgen), mAb TUB 2.1 against beta-tubulin (Sigma) and mAb 6.11.B.1 against acetylated tubulin (Sigma). Secondary antibodies used for immunofluorescence studies were coupled to Alexa 488 (Molecular Probes) or to Cy3 (Jackson ImmunoResearch Laboratories). Secondary antibodies used for western blotting were HRP-coupled pAbs from Jackson ImmunoResearch Laboratories.

Cell culture, transfection, treatment and immunofluorescence microscopy

COS-7 and HEK293 cells were cultured in DMEM medium supplemented with 10% fetal bovine serum and 1% penicillin-streptomycin (Invitrogen). Transient transfections were carried out with 3 μg of DNA using Exgen 500 reagent (Euromedex), according to the manufacturer's protocol. After 28 hours of transfection, cells were fixed for either 6 minutes in cold methanol at −20℃ or for 10 minutes in 4% paraformaldehyde. After paraformaldehyde fixation, cells were permeabilized with 0.05% saponin in PBS. For nocodazole treatment, transfected cells were incubated with 10 μM nocodazole (Sigma) for 30 minutes or 2 hours at 37℃, and either fixed directly with cold methanol (supplementary material Fig. S3), or lysed for 1 minute at 30℃ with OPT buffer (80 mM PIPES, pH 6.7, 1 mM EGTA, 1 mM $MgCl_2$, 0.5% Triton X-100, 10% glycerol) before fixation for Fig. 2D (Lieuvin et al., 1994). For Taxol treatment, transfected cells were treated with 40 μM Taxol (paclitaxel, Sigma) either immediately after transfection for 24 hours, or the day after transfection for 2 hours, and treated cells were fixed directly with cold methanol. For detection of Trisk 95 or 2C>A mutant of Trisk 95 at the cell surface, cells were fixed with paraformaldehyde and incubated with the guinea pig pAb against the C-terminus of Trisk 95, before being lysed with saponin and incubated with the rabbit pAb to the N-terminus of Trisk 95, and with secondary antibodies. Immunofluorescence preparations were observed under a Leica SPE confocal microscope.

Myoblasts were obtained from hind limb muscles of 2-day-old rats (Sprague-Dawley, Harlan; see below for procedures using animals). The cell-suspension was plated on 0.025% laminin-coated LabTek chambers (Nalge Nunc International). Cells were grown at 37℃ at 5% CO_2. After 2 days, cells were transfected with lipofectamine-Plus method and induced to differentiate with αMEM containing 2 mM L-glutamine, 100 μg/ml streptomycin, 100 U/ml penicillin, 1 mM sodium pyruvate, 1 mM dexamethasone, 50 mM hydrocortisone, supplemented with 10% heat-inactivated fetal bovine serum (all reagents from Bio-Whittaker) and 5% heat-inactivated horse serum (Biochrom).

Preparation of mouse muscle fibers for immunofluorescence microscopy

All procedures using animals were approved by the Institutional ethics committee and followed the guidelines of the National Research Council Guide for the care and use of laboratory animals. Flexor Digitorum Brevis (FDB) fibers were dissociated according to a procedure described (Pouvreau et al., 2007). Intact FDB muscles from the hind paw of a 3-month-old wild-type mouse were dissected in a Ringer-glucose solution (136 mm NaCl, 10 mm glucose, 5 mm KCl, 2.6 mm $CaCl_2$, 1 mm $MgCl_2$, 10 mm HEPES, pH 7.2) at 37℃. Dissected FDB were digested for 30–45 minutes at 37℃ in a solution of collagenase (2 mg/ml in Ringer-glucose, Sigma-Aldrich). Muscles were then rinsed for 10 minutes in Ringer-glucose at 37℃ and were dissociated by several flushing steps. Dissociated fibers were seeded on laminin-coated slides for 30 minutes at room temperature and were fixed for 6 minutes in cold methanol at −20℃. Fibers were permeabilized for 5 minutes with 1% Triton X-100 in PBS at room temperature, and saturated for 30 minutes with PBS supplemented with 0.1% Triton X-100, 0.5% bovine serum albumin and 2% goat serum. Fibers were then processed for immunofluorescence with antibodies described in the above section. Images of single confocal plane were captured on a Leica SPE confocal microscope.

Microtubule co-sedimentation assays

HEK293 cells were collected 28 hours after transfection and rinsed once in PBS and once in PEM buffer (PIPES 100 mM pH 6.8, EGTA 1 mM, $MgCl_2$ 1 mM) at 4℃. Cells were then lysed for 15 minutes at 4℃ in OPT buffer plus protease inhibitors. After three passages through a 29-gauge needle, samples were centrifuged at 20,000 ***g*** at 4℃ for 10 minutes. The supernatant of each sample was collected (Lysate sample, L) and incubated for 45 minutes at 37℃ with 40 μM paclitaxel (Sigma), 1 mM GTP, 5 mM $MgCl_2$ and 10 μM pure bovine tubulin (Caudron et al., 2000), to induce microtubule polymerization. Samples were layered onto a glycerol cushion (60% glycerol in PEM buffer) and then centrifuged at 100,000 ***g*** for 40 minutes at 20℃. Supernatant (S) over the glycerol cushion was collected before discarding the cushion. Pellet P1 was incubated for 20 minutes at 4℃ in PEM buffer supplemented with 5 mM $CaCl_2$ and 50 mM KCl, to induce microtubule disassembly before a second ultracentrifugation at 100,000 ***g***, for 20 minutes at 4℃ (Fourest-Lieuvin et al., 2006). After this second ultracentrifugation, the supernatant contained free tubulin and microtubule-associated proteins (MT fraction), whilst the pellet P2 corresponded mostly to protein aggregates. Samples were then processed for SDS-PAGE and western blotting.

Biotinylation of cell surface proteins

To biotinylate cell surface proteins, we used Sulfo-NHS-SS-Biotin (Thermo Scientific) according to manufacturer's protocol. Briefly, cells transfected with Trisk 95 or 2C>A mutant were washed twice with PBS at pH 8.0 and incubated with 800 μM Sulfo-NHS-SS-Biotin for 30 minutes at room temperature. Cells were then washed with 50 mM Tris at pH 8.0 to quench any non-reacted biotinylation reagent, and with ice-cold PBS at pH 7.4. Cells were lysed with RIPA buffer (25 mM Tris-HCl, pH 7.6, 150 mM NaCl, 1% NP-40, 1% sodium deoxycholate, 0.1% SDS) and lysates were incubated with streptavidin-agarose beads (Pierce) to bind biotinylated cell surface proteins. Cell surface protein (Mb) fraction was then separated from intracellular (IC) fraction, which was precipitated with chloroform and methanol. Whole lysates (L), Mb and IC fractions were loaded onto a gradient 5–15% gel for SDS-PAGE and western blotting.

Electron microscopy

COS-7 cells were transfected either with Trisk 95 or Trisk-95-GFP for 28 hours. For immunogold labeling, cells were fixed with 2% paraformaldehyde and 0.2% glutaraldehyde in phosphate buffer 0.1 M, pH 7.3 for 2 hours. Cells were then gently detached using a cell scraper, centrifuged at 1200 r.p.m. for 5 minutes and embedded in 10% gelatine. The cell pellet was then cut in 1 mm^3 pieces. These samples of cells were cryoprotected for 4 hours in 2.3 M sucrose and frozen in liquid nitrogen. Ultrathin cryosections of 40 nm were made at −120℃ using an ultra-cryo-microtome (Leica-Reichert) and retrieved with a 1:1 solution of 2.3 M sucrose and 2% methylcellulose according to the Tokuyasu protocol (Liou et al., 1996). Cryosections were first incubated with a rabbit pAb against GFP (Abcam) or the C-terminus of Trisk 95, and revealed with protein-A-gold particles (CMC, Utrecht). Labeled cryosections were viewed at 80 kV with a 1200EX JEOL TEM microscope and images were acquired with a digital camera (Veleta, SIS, Olympus).

For correlative electron microscopy, cells were cultured on a coverslip with a cell locate pattern made of carbon. The transfected cell of interest was localized by confocal microscopy and its position on the pattern was determined. Cells were then fixed with 2.5% glutaraldehyde in 0.1 M cacodylate buffer, pH 7.4, for 2 hours at room temperature, washed with cacodylate buffer and post-fixed with 1% osmium tetroxide in the same buffer for 1 hour at 4℃. After extensive washing with water, cells were stained with 1% uranyl acetate, pH 4, for 1 hour at 4℃. Cells were then dehydrated through graded alcohol (30%, 60%, 90%, 100%, 100%, 100%) and infiltrated with a 1:1 mix of Epon to 100% ethanol for 1 hour and incubated in fresh EPON (Flukka) for 3 hours. Finally, a capsule full of Epon was deposed on the surface of the cells and the resin was allowed to polymerize for 72 hours at 60℃. The polymerized block was then detached from the culture plate and ultrathin sections of the cell were cut with an ultramicrotome (Leica). Sections were post-stained with 4% uranyl acetate and 0.4% lead citrate before being observed under a transmission electron microscope at 80 kV as above.

FRAP on differentiated rat myotubes

FRAP experiments were performed by using a Zeiss LSM 510 Meta confocal microscope. Cells were imaged in LabTek chambers in medium containing 140 mM NaCl, 5 mM KCl, 10 mM glucose, 1 mM $MgCl_2$, 0.1 mM $CaCl_2$, 20 mM HEPES, and 0.4 mM EGTA. A 63× 1.4 NA Plan-Apochromat oil immersion objective (Zeiss) was used with a pinhole aperture of 4.96 Airy units. GFP was excited at 488 nm with an argon laser with low laser power (0.5%) and

emitted fluorescence collected with a long-pass 505 emission filter. After acquisition of ten prebleach images, photobleaching of GFP in a circular area 1.08 µm in diameter was performed by using the argon laser lines 458, 477 and 488 nm at 50% laser power and 50% transmission. Recovery of fluorescence in the bleached region was recorded every 50 mseconds over a period of 1–10 minutes until fluorescence level reached a plateau. Fluorescence intensities were acquired for the bleached region (I_{frap}), the whole cell (I_{whole}), and a background region (I_{base}). The data were low-pass 3×3 filtered with the Zeiss LSM 510 software for image noise reduction, and data analysis was performed by using macros designed in IgorPro software (WaveMetrics). The average fluorescence intensity within the bleached region was normalized to prebleach intensity for each time point and corrected for loss of fluorescence during acquisition. Fluorescence loss during acquisition was no more than 10%. The normalized data were fitted by the exponential equation: $I_{frap\text{-}est}(t) = A(1-e^{-\tau_1 t})$, where A represents the mobile fraction. Fitting quality was evaluated by the probability Q value and accepted when $Q>0.01$. Statistical analyses were performed by using Instat Software (GraphPad).

Quantifications and statistics

Relative expression levels of Trisk 95 in cells were quantified on single focal plane images taken with a Leica SPE confocal microscope, by tracing the entire outline of the Trisk-95-labeled ER and measuring the average fluorescence intensities for each outline using ImageJ software (version 1.44i, NIH). A total of 45 cells from two separate experiments were quantified (Fig. 1B). Thickness of the Trisk-95-associated tubules and of the control ER was measured on electron microscopy images by using the morphometric tool of the iTEM software. At least 40 transfected and non-transfected cells were quantified on four non-consecutive ultrathin cryosections. For quantifications in Figs 2,4,5, non-transfected cells (control) or transfected cells presenting one peculiar phenotype, e.g. disorganized microtubules or ER rope-like structures, were directly counted under a fluorescence Leica microscope. At least three separate experiments were performed, and at least 200 cells were counted in each experiment. For quantifications in Fig. 7, see above section on FRAP studies. Statistics were performed using Student's *t*-test on Prism 4.0 software (GraphPad), with n = number of cells in Fig. 1B, number of experiments in Figs 2,4,5 and number of clusters in Fig. 7.

Acknowledgements

We thank Melina Petrel for technical help.

Funding

This work was supported by grants from Association Française contre les Myopathies (AFM) and Agence Nationale de la Recherche (ANR-Maladies rares).

Supplementary material available online at
http://jcs.biologists.org/lookup/suppl/doi:10.1242/jcs.100958/-/DC1

References

Block, B. A., O'Brien, J. and Meissner, G. (1994). Characterization of the sarcoplasmic reticulum proteins in the thermogenic muscles of fish. *J. Cell Biol.* **127**, 1275-1287.

Brandt, N. R., Caswell, A. H., Wen, S. R. and Talvenheimo, J. A. (1990). Molecular interactions of the junctional foot protein and dihydropyridine receptor in skeletal muscle triads. *J. Membr. Biol.* **113**, 237-251.

Caudron, N., Valiron, O., Usson, Y., Valiron, P. and Job, D. (2000). A reassessment of the factors affecting microtubule assembly and disassembly in vitro. *J. Mol. Biol.* **297**, 211-220.

Cusimano, V., Pampinella, F., Giacomello, E. and Sorrentino, V. (2009). Assembly and dynamics of proteins of the longitudinal and junctional sarcoplasmic reticulum in skeletal muscle cells. *Proc. Natl. Acad. Sci. USA* **106**, 4695-4700.

Felder, E., Protasi, F., Hirsch, R., Franzini-Armstrong, C. and Allen, P. D. (2002). Morphology and molecular composition of sarcoplasmic reticulum surface junctions in the absence of DHPR and RyR in mouse skeletal muscle. *Biophys. J.* **82**, 3144-3149.

Flucher, B. E. (1992). Structural analysis of muscle development: transverse tubules, sarcoplasmic reticulum, and the triad. *Dev. Biol.* **154**, 245-260.

Flucher, B. E. and Franzini-Armstrong, C. (1996). Formation of junctions involved in excitation-contraction coupling in skeletal and cardiac muscle. *Proc. Natl. Acad. Sci. USA* **93**, 8101-8106.

Flucher, B. E., Phillips, J. L., Powell, J. A., Andrews, S. B. and Daniels, M. P. (1992). Coordinated development of myofibrils, sarcoplasmic reticulum and transverse tubules in normal and dysgenic mouse skeletal muscle, in vivo and in vitro. *Dev. Biol.* **150**, 266-280.

Fourest-Lieuvin, A., Peris, L., Gache, V., Garcia-Saez, I., Juillan-Binard, C., Lantez, V. and Job, D. (2006). Microtubule regulation in mitosis: tubulin phosphorylation by the cyclin-dependent kinase Cdk1. *Mol. Biol. Cell* **17**, 1041-1050.

Froemming, G. R., Murray, B. E. and Ohlendieck, K. (1999). Self-aggregation of triadin in the sarcoplasmic reticulum of rabbit skeletal muscle. *Biochim. Biophys. Acta* **1418**, 197-205.

Gómez, A. M., Kerfant, B. G. and Vassort, G. (2000). Microtubule disruption modulates Ca(2+) signaling in rat cardiac myocytes. *Circ. Res.* **86**, 30-36.

Hong, T. T., Smyth, J. W., Gao, D., Chu, K. Y., Vogan, J. M., Fong, T. S., Jensen, B. C., Colecraft, H. M. and Shaw, R. M. (2010). BIN1 localizes the L-type calcium channel to cardiac T-tubules. *PLoS Biol.* **8**, e1000312.

Ito, K., Komazaki, S., Sasamoto, K., Yoshida, M., Nishi, M., Kitamura, K. and Takeshima, H. (2001). Deficiency of triad junction and contraction in mutant skeletal muscle lacking junctophilin type 1. *J. Cell Biol.* **154**, 1059-1068.

Kim, K. C., Caswell, A. H., Talvenheimo, J. A. and Brandt, N. R. (1990). Isolation of a terminal cisterna protein which may link the dihydropyridine receptor to the junctional foot protein in skeletal muscle. *Biochemistry* **29**, 9281-9289.

Klopfenstein, D. R., Kappeler, F. and Hauri, H. P. (1998). A novel direct interaction of endoplasmic reticulum with microtubules. *EMBO J.* **17**, 6168-6177.

Klopfenstein, D. R., Klumperman, J., Lustig, A., Kammerer, R. A., Oorschot, V. and Hauri, H. P. (2001). Subdomain-specific localization of CLIMP-63 (p63) in the endoplasmic reticulum is mediated by its luminal alpha-helical segment. *J. Cell Biol.* **153**, 1287-1300.

Kobayashi, Y. M., Alseikhan, B. A. and Jones, L. R. (2000). Localization and characterization of the calsequestrin-binding domain of triadin 1. Evidence for a charged beta-strand in mediating the protein-protein interaction. *J. Biol. Chem.* **275**, 17639-17646.

Lee, E., Marcucci, M., Daniell, L., Pypaert, M., Weisz, O. A., Ochoa, G. C., Farsad, K., Wenk, M. R. and De Camilli, P. (2002). Amphiphysin 2 (Bin1) and T-tubule biogenesis in muscle. *Science* **297**, 1193-1196.

Lee, J. M., Rho, S. H., Shin, D. W., Cho, C., Park, W. J., Eom, S. H., Ma, J. and Kim, D. H. (2004). Negatively charged amino acids within the intraluminal loop of ryanodine receptor are involved in the interaction with triadin. *J. Biol. Chem.* **279**, 6994-7000.

Lieuvin, A., Labbé, J. C., Dorée, M. and Job, D. (1994). Intrinsic microtubule stability in interphase cells. *J. Cell Biol.* **124**, 985-996.

Liou, W., Geuze, H. J. and Slot, J. W. (1996). Improving structural integrity of cryosections for immunogold labeling. *Histochem. Cell Biol.* **106**, 41-58.

Marty, I., Robert, M., Villaz, M., De Jongh, K., Lai, Y., Catterall, W. A. and Ronjat, M. (1994). Biochemical evidence for a complex involving dihydropyridine receptor and ryanodine receptor in triad junctions of skeletal muscle. *Proc. Natl. Acad. Sci. USA* **91**, 2270-2274.

Marty, I., Robert, M., Ronjat, M., Bally, I., Arlaud, G. and Villaz, M. (1995). Localization of the N-terminal and C-terminal ends of triadin with respect to the sarcoplasmic reticulum membrane of rabbit skeletal muscle. *Biochem. J.* **307**, 769-774.

Marty, I., Thevenon, D., Scotto, C., Groh, S., Sainnier, S., Robert, M., Grunwald, D. and Villaz, M. (2000). Cloning and characterization of a new isoform of skeletal muscle triadin. *J. Biol. Chem.* **275**, 8206-8212.

Marty, I., Fauré, J., Fourest-Lieuvin, A., Vassilopoulos, S., Oddoux, S. and Brocard, J. (2009). Triadin: what possible function 20 years later? *J. Physiol.* **587**, 3117-3121.

Nicot, A. S., Toussaint, A., Tosch, V., Kretz, C., Wallgren-Pettersson, C., Iwarsson, E., Kingston, H., Garnier, J. M., Biancalana, V., Oldfors, A. et al. (2007). Mutations in amphiphysin 2 (BIN1) disrupt interaction with dynamin 2 and cause autosomal recessive centronuclear myopathy. *Nat. Genet.* **39**, 1134-1139.

Oddoux, S., Brocard, J., Schweitzer, A., Szentesi, P., Giannesini, B., Brocard, J., Fauré, J., Pernet-Gallay, K., Bendahan, D., Lunardi, J. et al. (2009). Triadin deletion induces impaired skeletal muscle function. *J. Biol. Chem.* **284**, 34918-34929.

Paolini, C., Quarta, M., Nori, A., Boncompagni, S., Canato, M., Volpe, P., Allen, P. D., Reggiani, C. and Protasi, F. (2007). Reorganized stores and impaired calcium handling in skeletal muscle of mice lacking calsequestrin-1. *J. Physiol.* **583**, 767-784.

Park, S. H. and Blackstone, C. (2010). Further assembly required: construction and dynamics of the endoplasmic reticulum network. *EMBO Rep.* **11**, 515-521.

Park, S. H., Zhu, P. P., Parker, R. L. and Blackstone, C. (2010). Hereditary spastic paraplegia proteins REEP1, spastin, and atlastin-1 coordinate microtubule interactions with the tubular ER network. *J. Clin. Invest.* **120**, 1097-1110.

Pouvreau, S., Royer, L., Yi, J., Brum, G., Meissner, G., Ríos, E. and Zhou, J. (2007). Ca(2+) sparks operated by membrane depolarization require isoform 3 ryanodine receptor channels in skeletal muscle. *Proc. Natl. Acad. Sci. USA* **104**, 5235-5240.

Prins, K. W., Humston, J. L., Mehta, A., Tate, V., Ralston, E. and Ervasti, J. M. (2009). Dystrophin is a microtubule-associated protein. *J. Cell Biol.* **186**, 363-369.

Ralston, E., Lu, Z. and Ploug, T. (1999). The organization of the Golgi complex and microtubules in skeletal muscle is fiber type-dependent. *J. Neurosci.* **19**, 10694-10705.

Realini, C., Rogers, S. W. and Rechsteiner, M. (1994). KEKE motifs. Proposed roles in protein-protein association and presentation of peptides by MHC class I receptors. *FEBS Lett.* **348**, 109-113.

Renken, C., Hsieh, C. E., Marko, M., Rath, B., Leith, A., Wagenknecht, T., Frank, J. and Mannella, C. A. (2009). Structure of frozen-hydrated triad junctions: a case study in motif searching inside tomograms. *J. Struct. Biol.* **165**, 53-63.

Rezgui, S. S., Vassilopoulos, S., Brocard, J., Platel, J. C., Bouron, A., Arnoult, C., Oddoux, S., Garcia, L., De Waard, M. and Marty, I. (2005). Triadin (Trisk 95) overexpression blocks excitation-contraction coupling in rat skeletal myotubes. *J. Biol. Chem.* **280**, 39302-39308.

Shen, X., Franzini-Armstrong, C., Lopez, J. R., Jones, L. R., Kobayashi, Y. M., Wang, Y., Kerrick, W. G., Caswell, A. H., Potter, J. D., Miller, T. et al. (2007).

Triadins modulate intracellular Ca(2+) homeostasis but are not essential for excitation-contraction coupling in skeletal muscle. *J. Biol. Chem.* **282**, 37864-37874.

Shibata, Y., Voss, C., Rist, J. M., Hu, J., Rapoport, T. A., Prinz, W. A. and Voeltz, G. K. (2008). The reticulon and DP1/Yop1p proteins form immobile oligomers in the tubular endoplasmic reticulum. *J. Biol. Chem.* **283**, 18892-18904.

Shibata, Y., Hu, J., Kozlov, M. M. and Rapoport, T. A. (2009). Mechanisms shaping the membranes of cellular organelles. *Annu. Rev. Cell Dev. Biol.* **25**, 329-354.

Shibata, Y., Shemesh, T., Prinz, W. A., Palazzo, A. F., Kozlov, M. M. and Rapoport, T. A. (2010). Mechanisms determining the morphology of the peripheral ER. *Cell* **143**, 774-788.

Takeshima, H., Komazaki, S., Nishi, M., Iino, M. and Kangawa, K. (2000). Junctophilins: a novel family of junctional membrane complex proteins. *Mol. Cell* **6**, 11-22.

Thevenon, D., Smida-Rezgui, S., Chevessier, F., Groh, S., Henry-Berger, J., Beatriz Romero, N., Villaz, M., DeWaard, M. and Marty, I. (2003). Human skeletal muscle triadin: gene organization and cloning of the major isoform, Trisk 51. *Biochem. Biophys. Res. Commun.* **303**, 669-675.

Vassilopoulos, S., Thevenon, D., Rezgui, S. S., Brocard, J., Chapel, A., Lacampagne, A., Lunardi, J., Dewaard, M. and Marty, I. (2005). Triadins are not triad-specific proteins: two new skeletal muscle triadins possibly involved in the architecture of sarcoplasmic reticulum. *J. Biol. Chem.* **280**, 28601-28609.

Vedrenne, C. and Hauri, H. P. (2006). Morphogenesis of the endoplasmic reticulum: beyond active membrane expansion. *Traffic* **7**, 639-646.

Wang, Y., Li, X., Duan, H., Fulton, T. R., Eu, J. P. and Meissner, G. (2009). Altered stored calcium release in skeletal myotubes deficient of triadin and junctin. *Cell Calcium* **45**, 29-37.